

Low-rank multi-parametric covariance identification^{*}

Antoni Musolas[†] Estelle Massart[‡] Julien M. Hendrickx[§] P.-A. Absil[§]

Youssef Marzouk[†]

April 28, 2020

Abstract

We propose a differential geometric construction for families of low-rank covariance matrices, via interpolation on low-rank matrix manifolds. In contrast with standard parametric covariance classes, these families offer significant flexibility for problem-specific tailoring via the choice of “anchor” matrices for the interpolation. Moreover, their low-rank facilitates computational tractability in high dimensions and with limited data. We employ these covariance families for both interpolation and identification, where the latter problem comprises selecting the most representative member of the covariance family given a data set. In this setting, standard procedures such as maximum likelihood estimation are nontrivial because the covariance family is rank-deficient; we resolve this issue by casting the identification problem as distance minimization. We demonstrate the power of these differential geometric families for interpolation and identification in a practical application: wind field covariance approximation for unmanned aerial vehicle navigation.

Keywords: covariance approximation, geodesic, low-rank covariance function, positive-semidefinite matrices, Riemannian metric, optimization on manifolds, maximum likelihood

AMS: 53C22, 62J10

1 Introduction

One of the most fundamental problems in multivariate analysis and uncertainty quantification is the construction of covariance matrices. Covariance matrices are an essential tool in climatology, econometrics, model order reduction, biostatistics, signal processing, and geostatistics, among other applications. As a specific example (which we shall revisit in this paper), covariance matrices of wind velocity fields [33, 34, 40, 8] capture the relationships among wind velocity components at different points in space. These relationships enable recursive approximation

^{*}This work was supported by (i) “la Caixa” Banking Foundation (ID 100010434) under project LCF/BQ/AN13/10280009, (ii) the Fonds de la Recherche Scientifique (FNRS) and the Fonds Wetenschappelijk Onderzoek (FWO) – Vlaanderen under EOS (Project 30468160), (iii) the “Communauté française de Belgique – Actions de Recherche Concertées” (Contract ARC 14/19-060), (iv) the WBI-World Excellence Fellowship, (v) the United States Department of Energy, Office of Advanced Scientific Computing Research (ASCR). The second author is supported by the National Physical Laboratory and the Alan Turing Institute. Most of the work was done when the second author was with ICTEAM, UCLouvain, Belgium.

[†]Center for Computational Science & Engineering, Massachusetts Institute of Technology, Cambridge, MA USA (musolas@mit.edu, ymarz@mit.edu).

[‡]Mathematical Institute, University of Oxford, OX2 6GG, UK (estelle.massart@maths.ox.ac.uk).

[§]ICTEAM Institute, UCLouvain, Avenue Georges Lemaître 4 bte L4.05.01, 1348 Louvain-la-Neuve, Belgium, (julien.hendrickx@uclouvain.be, pa.absil@uclouvain.be)

or updating of the wind field as new pointwise measurements become available. Similarly, in oil reservoirs [47, 48], covariance matrices allow information from borehole measurements to be propagated into more accurate global estimates of the permeability field. In telecommunications [39], covariance matrices and their eigenvectors are paramount for discerning between signal and noise.

Widely used methods in spatial statistics [14, 52, 57] include variogram estimation [13, 11] (often a first step in kriging [56, 17, 24]) or tapering of sample covariance matrices [23, 19]. Other regularized covariance estimation methodologies include sparse covariance and precision matrix estimation [6, 18, 7] and many varieties of shrinkage [35, 36, 55, 37]. Many of these methods make rather generic assumptions on the covariance matrix (e.g., sparsity of the precision, or some structure in the spectrum); others (e.g., Matérn covariance kernels or particular variogram models) assume that the covariance is described within some parametric family. The latter can make the estimation problem quite tractable, even with relatively limited data, since the number of degrees of freedom in the family may be small.

Unfortunately, standard parametric covariance families (e.g., Matérn) [12, 51, 53] can be insufficiently flexible for practical applications. For instance, in wind field modeling, these covariance families are insufficiently expressive to capture the non-stationary and multiscale features of the velocity or vorticity [30, 31, 32]. Nonparametric approaches such as sparse precision estimation may be less restrictive, but neither approach easily allows prior knowledge—such as known wind covariances at other conditions—to be incorporated. Moreover, most of these methods yield full-rank covariance matrices, which are impractical for high-dimensional problems. For example, direct manipulation of full-rank covariances in high dimensional settings might preclude recursive estimation (i.e., conditioning) from being performed online.

In this paper, we propose to build parametric covariance functions from piecewise-Bézier interpolation techniques on manifolds, using representative covariance matrices as anchors. (See [46] for a related approach using full-rank geodesics.) These covariance functions offer significant flexibility for problem-specific tailoring and can be reduced to any given rank; both of these features enable broad applicability. We use our proposed covariance functions for identification—finding the most representative member of a family given a data set—and interpolation—given anchors at known or “labeled” conditions, predicting covariance matrices at new conditions between those of the anchors. Observe that these objectives do not require an appeal to asymptotic statistical properties, which are not investigated here.

Interpolation on matrix manifolds has been an active research topic in the last few years; see, e.g., [5, 54, 25, 28, 9]. Here we propose to rely on piecewise-Bézier curves and surfaces on manifolds that have been investigated, e.g., in [2, 3, 21, 45]. As for the space to interpolate on, an immediate choice would have been the set of all $n \times n$ covariance matrices, namely the set of $n \times n$ symmetric positive-semidefinite (PSD) matrices; however this set is not a manifold. (Specifically, it is not a submanifold of $\mathbb{R}^{n \times n}$.) Instead, we will consider the set of $n \times n$ covariance matrices of fixed rank r , which is known to be a manifold; see, e.g., [59]. Among others, [50] and [44] investigated the full-rank case ($r = n$) and pioneered building matrix functions using geodesics on the manifold of symmetric positive-definite (SPD) matrices. For the low-rank case ($r < n$), several geometries are available [4, 59, 60]. We will resort to the geometry proposed in [26] and further developed in [41], as it has the crucial advantage of providing a closed-form expression for the endpoint geodesic problem, which appears as a pervasive subproblem in Bézier-type interpolation techniques on manifolds.

We point out that univariate interpolation on the manifold of fixed-rank PSD matrices has already been applied, e.g., to the wind field approximation problem in [22], to protein conformation in [38], to computer vision and facial recognition in [27, 58], and to parametric model order reduction in [42]. The present work is, to our knowledge, a first step towards the multivariate

case.

There are three original contributions in this paper. First, we devise new *low-rank* parameterized covariance families, based on given problem-specific anchor covariance matrices. The rank of the anchor matrices is assumed to be equal to some value r , usually much smaller than the size n of the matrices. The resulting covariance families are shown to contain only matrices of rank less than or equal to r . In high-dimensional applications, this allows reducing the computational cost of matrix manipulations, while still explaining the majority of the variance of the data. Working with low-rank covariance families also results in robustness to *small* data. Second, we propose minimization of an appropriate loss function as an alternative to maximum likelihood estimation for selecting the most representative member of this covariance family given some data. When the covariance family is low-rank, maximum likelihood estimation is not trivial, as the probability density of the data (assumed Gaussian) is degenerate. Third, we demonstrate the previous two points in an application: wind field velocity characterization for UAV navigation. We notice that when connecting anchors labeled with different values of the prevailing wind conditions, the values in between correspond to intermediate wind conditions.

The rest of this paper is organized as follows. We summarize the tools needed to work on the manifold of fixed-rank PSD matrices in Section 2. We introduce our new covariance functions in Section 3, for both the one- and the multi-parameter cases. In Section 4, we present methods to solve the covariance identification problem via distance minimization. In Section 5, we illustrate the behaviors of the different covariance functions on a case study: wind field approximation.

2 The geometry of the set of positive-semidefinite matrices

In this section, we define useful tools to work on the manifold $\mathcal{S}_+(r, n)$ of positive-semidefinite (PSD) matrices, with rank r and size $n \times n$, with $r < n$.

Several metrics have been proposed for this manifold but, to our knowledge, none of them manages to turn it into a complete metric space with a closed-form expression for endpoint geodesics. We use the quotient geometry $\mathcal{S}_+(r, n) \simeq \mathbb{R}_*^{n \times r} / \mathcal{O}(r)$ proposed in [26] and further developed in [41], with $\mathbb{R}_*^{n \times r}$ endowed with the Euclidean metric. This geometry relies on the fact that a matrix $A \in \mathcal{S}_+(r, n)$ can be factorized as $A = Y_A Y_A^\top$, where the factor $Y_A \in \mathbb{R}_*^{n \times r}$ has full column rank. The decomposition is not unique, as each factor $S_A = Y_A Q$, with $Q \in \mathcal{O}(r)$ an orthogonal matrix, leads to the same product. As a consequence, any PSD matrix A is represented by an equivalence class:

$$[Y_A] = \{Y_A Q | Q \in \mathcal{O}(r)\}.$$

In our computations, we work with representatives of the equivalence classes. For example, the geodesic between two PSD matrices A and B will be computed based on two arbitrary representatives Y_A, Y_B , of the corresponding equivalence classes. The geodesic will of course be invariant to the choice of the representatives. Moreover, this approach saves computational cost as the representatives are of size $n \times r$, instead of $n \times n$.

In [41], the authors propose an expression for the main tools to perform computations on $\mathcal{S}_+(r, n)$, endowed with this geometry. The geodesic $\varphi_{A_1 \rightarrow A_2}$ between two PSD matrices A_1, A_2 , with representatives Y_{A_1} and Y_{A_2} , is given by:

$$\varphi_{A_1 \rightarrow A_2}(t) = Y_{\varphi_{A_1 \rightarrow A_2}(t)} Y_{\varphi_{A_1 \rightarrow A_2}(t)}^\top \quad \text{with} \quad Y_{\varphi_{A_1 \rightarrow A_2}(t)} = Y_{A_1} + t \dot{Y}_{A_1 \rightarrow A_2}. \quad (1)$$

In this expression, the vector $\dot{Y}_{A_1 \rightarrow A_2}$ is defined as $\dot{Y}_{A_1 \rightarrow A_2} = Y_{A_2} Q^\top - Y_{A_1}$ with $Y_{A_1}^\top Y_{A_2} = H Q$ a polar decomposition. In the generic case where $Y_{A_1}^\top Y_{A_2}$ is nonsingular, the polar decomposition is

unique and the resulting curve $t \in [0, 1] \mapsto \varphi_{A_1 \rightarrow A_2}(t)$ is the unique minimizing geodesic between A_1 and A_2 . This curve has the following properties:

1. $\varphi_{A_1 \rightarrow A_2}(0) = A_1$, and $\varphi_{A_1 \rightarrow A_2}(1) = A_2$.
2. For each $t \in \mathbb{R}$, $\varphi_{A_1 \rightarrow A_2}(t) \in \mathcal{S}_+(\leq r, n)$,

where the notation $\mathcal{S}_+(\leq r, n)$ stands for the set of positive-semidefinite matrices of rank upper-bounded by r .

Notice that the last property suggests that this manifold is not a complete metric space for this metric, because the points in the geodesics are not necessarily of rank r . However, completeness is not central for statistical modeling, and, as we will see in Section 5, the fact that not all covariance matrices have the same rank will not have any consequence in practice.

We finally mention that [41] also contains expressions for the exponential and logarithm maps, on which rely the patchwise Bézier surfaces introduced in Section 3.3.2 below. Referring to the PSD matrices discussed above (e.g., A_1, A_2) as “data matrices,” we make the following assumption:

Hypothesis 1 *The data matrices are such that all the logarithm and exponential maps to which we refer in the sequel are well-defined.*

Hypothesis 1 will typically be satisfied when the data matrices are sufficiently close to each other; see [41] for more information.

Instead of working directly on the quotient manifold (which involves the computation of geodesics, exponential and logarithm maps), a simpler approach consists in working on an affine section of the quotient. Consider an equivalence class $[Y_A]$ with Y_A a representative of the class. We define the section of the quotient at Y_A as the set of points:

$$\mathcal{S}_A := \{Y_A (I + (Y_A^\top Y_A)^{-1} S) + Y_{A\perp} K \mid S^\top = S, S \succ -Y_A^\top Y_A, K \in \mathbb{R}^{(n-r) \times r}\}, \quad (2)$$

where the matrix $Y_{A\perp} \in \mathbb{R}^{n \times (n-r)}$ is any orthonormal basis for the orthogonal complement of Y_A , i.e., $Y_A^\top Y_{A\perp} = 0$ and $Y_{A\perp}^\top Y_{A\perp} = I_{n-r}$. The constraint $S \succ -Y_A^\top Y_A$ guarantees that there is at most one representative of each equivalence class $[Y_B]$ in the section, and exactly one under the generic condition that $Y_A^\top Y_B$ is nonsingular.

Consider the section of the quotient at Y_{A_1} . The representative in the section of any equivalence class $[Y_{A_2}]$ (with $Y_{A_1}^\top Y_{A_2}$ nonsingular) is then $\bar{Y}_{A_2} = Y_{A_2} Q^\top$, where Q is the orthogonal factor of the polar decomposition of $Y_{A_1}^\top Y_{A_2}$. Once all the points are projected on the section, we can simply perform Euclidean operations on the section.

3 Construction of low-rank covariance functions

A low-rank covariance function is a mapping from a set of parameters to a low-rank PSD matrix.

Definition 1 (Low-rank covariance function and family) *A p -parameter low-rank covariance function is a map $\varphi : \mathbb{R}^p \rightarrow \cup_{k=0}^r \mathcal{S}_+(k, n)$, for $r < n$; its corresponding covariance family is the image of φ .*

3.1 First-order covariance functions

In this section, we consider two possible generalizations of multilinear interpolation to manifolds. The simplest way consists in mapping all the points to a linear approximation of the manifold (here, a section of the quotient), and applying multilinear interpolation on the section. A second approach resorts to the geodesics (generalization of straight lines) on the manifold. It is interesting to notice that both reduce to the one-parameter geodesic eq. (1) in the one-parameter case if the reference point of the section belongs to the geodesic (cf. Remark 1).

3.1.1 First-order sectional covariance function

The main idea is to consider a section eq. (2), projecting the data matrices to that section and performing multilinear interpolation on it. The definition below presents the sectional covariance function in the case of bilinear interpolation: we explain the steps to obtain it. A schematic representation can be seen in Figure 1.

Definition 2 (The sectional p -parameter covariance function) *The sectional p -parameter covariance function is obtained as follows:*

1. Select a member \bar{Y}_{A_1} of the equivalence class $[Y_{A_1}]$.
2. Intersect the equivalence classes of p data matrices ($Y_{A_i}, i = 1 \dots p$) with the section defined by \bar{Y}_{A_1} to obtain:

$$\bar{Y}_{A_i}, i = 1 \dots p.$$

3. Perform any type of Euclidean multilinear interpolation of the projected data matrices. For instance, in the bilinear case (two parameter and four data matrices):

$$\bar{Y}_{\varphi_{A_1 \rightarrow \dots \rightarrow A_4}}(t_1, t_2) = \bar{Y}_{A_1}(1 - t_1)(1 - t_2) + \bar{Y}_{A_2}(1 - t_1)t_2 + \bar{Y}_{A_3}t_1(1 - t_2) + \bar{Y}_{A_4}t_1t_2.$$

4. Multiply the factor by its transpose to obtain the full matrix:

$$\varphi_{A_1 \rightarrow A_2 \rightarrow A_3 \rightarrow A_4}(t_1, t_2) = \bar{Y}_{\psi_{A_1 \rightarrow A_2 \rightarrow A_3 \rightarrow A_4}}(t_1, t_2) \bar{Y}_{\psi_{A_1 \rightarrow A_2 \rightarrow A_3 \rightarrow A_4}}^\top(t_1, t_2).$$

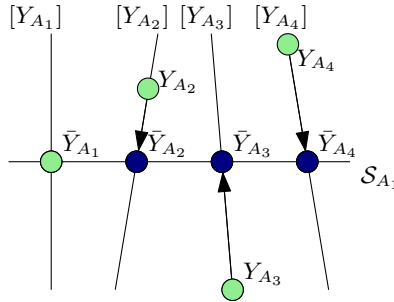


Figure 1: Schematic representation of the sectional covariance function. The vertical lines correspond to equivalence classes and the horizontal line is the section into which the data matrices are projected.

3.1.2 First-order geodesic covariance function

By connecting p geodesics of the form in eq. (1), we can obtain the *geodesic* p -parameter covariance function, which is described below and represented in Section 3.1.2.

Definition 3 (The *geodesic* p -parameter covariance function) *By connecting two one-parameter geodesics, we obtain the geodesic two-parameter covariance function:*

$$\varphi_{(A_1 \rightarrow A_2) \rightarrow (A_3 \rightarrow A_4)}(t_1, t_2) := \varphi_{(\varphi_{A_1 \rightarrow A_2}(t_1)) \rightarrow (\varphi_{A_3 \rightarrow A_4}(t_1))}(t_2). \quad (3)$$

Recursively, we can construct the geodesic p -parameter covariance function.

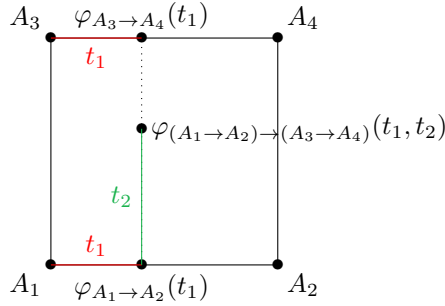


Figure 2: Configuration of the points in a Euclidean setting. Example for two parameters.

In order to build a geodesic p -parameter covariance function, according to the definition, we need 2^p data matrices.

Remark 1 *For the one-parameter case, if the reference point of the section is on the geodesic, the sectional and geodesic families coincide. Indeed, using the relationships from Section 2, notice that the geodesic (geodesic one-parameter function) can be converted to a sectional one-parameter covariance function:*

$$\begin{aligned} Y_{\varphi_{A_1 \rightarrow A_2}}(t) &= Y_{A_1} + t\dot{Y}_{A_1 \rightarrow A_2} = Y_{A_1} + t(Y_{A_2}Q^\top - Y_{A_1}) = Y_{A_1}(1 - t) + tY_{A_2}Q^\top \\ &= Y_{A_1}(1 - t) + t\bar{Y}_{A_2}, \end{aligned}$$

where $\bar{Y}_{A_2} = Y_{A_2}Q^\top$ is the projection of Y_{A_2} into the section defined by Y_{A_1} .

3.2 Piecewise first-order covariance functions

In practical applications, it is desirable to build covariance functions by patches. Each patch only depends on a reduced number of data matrices, usually those that are “closest” in some sense. Let us illustrate using patches of two-parameter covariance functions. We assume that the data matrices used to define the family (equivalently called the “anchor” covariance matrices) are described by a grid of indices: this collection consists of matrices $(A_{i,j})$, with $A_{i,j} \in \mathcal{S}_+(r, n)$, and with $i \in \{0, \dots, N_1\}$ and $j \in \{0, \dots, N_2\}$. The two covariance families proposed in the previous section can be computed on each patch of the grid, to build patchwise multilinear surfaces. The resulting surfaces will be denoted φ^{LS} and φ^{LG} , where the L stands for Linear (those surfaces were obtained as generalization of linear interpolation on manifolds), the S for Section, and the G for Geodesic.

Definition 4 Given a grid of points $(A_{i,j})$, with $A_{i,j} \in \mathcal{S}_+(r, n)$, and with $i \in \{0, 1, \dots, N_1\}$ and $j \in \{0, 1, \dots, N_2\}$, the first-order patchwise surfaces $\varphi^{\text{LS}} : [0, N_1] \times [0, N_2] \rightarrow \mathcal{S}_+(\leq r, n)$ and $\varphi^{\text{LG}} : [0, N_1] \times [0, N_2] \rightarrow \mathcal{S}_+(\leq r, n)$ are respectively the unions of the surfaces $\varphi_{l,m}^{\text{LS}}$ and $\varphi_{l,m}^{\text{LG}}$, each defined as follows. Let $l = 0, \dots, N_1 - 1$ and $m = 0, \dots, N_2 - 1$ be the indices of a patch. The function $\varphi_{l,m}^{\text{LS}}$, delimited by the data matrices $A_{l,m}, A_{l+1,m}, A_{l,m+1}, A_{l+1,m+1}$, is the sectional two-parameter covariance function defined in Definition 2, with bilinear interpolation of the representatives of the points $A_{l,m}, A_{l+1,m}, A_{l,m+1}, A_{l+1,m+1}$ in the section chosen for that patch. Examples of choices of sections are given in Section 5.

The function $\varphi_{l,m}^{\text{LG}}$ is the geodesic two-parameter covariance function, defined in Definition 3, that interpolates the points $A_{l,m}, A_{l+1,m}, A_{l,m+1}, A_{l+1,m+1}$.

Proposition 1 If for each patch, the data matrices located on the corners of the patch satisfy Hypothesis 1, it holds, except possibly for a zero measure set, that $\varphi^{\text{LS}}(t_1, t_2) \in \mathcal{S}_+(r, n)$ and $\varphi^{\text{LG}}(t_1, t_2) \in \mathcal{S}_+(r, n)$.

Proof: For $s \in \{LS, LG\}$, and for $(t_1, t_2) \in [0, 1] \times [0, 1]$, let $Y_\varphi^s(t_1, t_2)$ be a representative of the equivalence class associated with $\varphi^s(t_1, t_2)$. Consider the function $f : [0, 1] \times [0, 1] \rightarrow \mathbb{R} : (t_1, t_2) \mapsto \det(Y_\varphi^s(t_1, t_2)^\top Y_\varphi^s(t_1, t_2))$. This function is zero if and only if $\varphi^s(t_1, t_2)$ has rank $k < r$. Moreover, under Hypothesis 1, this function is real analytic. Indeed, in the case $s = LS$, it is a polynomial in t_1 and t_2 , which is real analytic. In the case $s = LG$, it can be readily checked that:

$$Y_\varphi^s = (1 - t_1)(1 - t_2)Y_{A_1} + t_1(1 - t_2)Y_{A_2}Q_{1-2}^\top + (1 - t_1)t_2Y_{A_3}Q(t_1)^\top + t_1t_2Y_{A_4}Q_{3-4}^\top Q(t_1)^\top,$$

where Q_{1-2} (resp. Q_{3-4}) is the orthogonal factor of the polar decomposition of $Y_{A_1}^\top Y_{A_2}$ (resp. $Y_{A_3}^\top Y_{A_4}$), and $Q(t_1)$ is the orthogonal factor of the polar decomposition of the matrix $M := ((1 - t_1)Y_{A_1} + t_1Y_{A_2}Q_{1-2}^\top)^\top((1 - t_1)Y_{A_3} + t_1Y_{A_4}Q_{3-4}^\top)$; see [41] for more information. If Hypothesis 1 holds, this matrix is nonsingular for all $t_1 \in [0, 1]$ [41]. The polar decomposition of a one-variable matrix function $t_1 \mapsto M(t_1)$, with $M(t_1)$ nonsingular, is real analytic [43, Theorem 3]. We then conclude the proof using the fact that the set of zeros of a real analytic function $f : \mathbb{R}^n \rightarrow \mathbb{R}$ has measure zero; see, e.g., [29, Remark 5.23]. \square

3.3 Higher-order covariance functions using Bézier curves

The previous section presented two families defined as generalizations of multilinear interpolation on the manifold. In this section, we consider higher-order interpolation on the manifold. We focus on patchwise Bézier surfaces on the grid. Again, we will distinguish two cases: methods resorting to Euclidean algorithms in a section of the manifold and methods based on successive evaluations of geodesics.

3.3.1 Higher-order sectional covariance function

This method consists in first projecting all the data matrices on a section of the manifold (cf. Equation (2)), and then using a classical Euclidean Bézier interpolation algorithm in the section.

We focus on patchwise cubic Bézier surfaces. Those surfaces are defined by a set of control points $(b_{i,j})_{i,j=0,\dots,3}$, with $b_{i,j} \in \mathbb{R}^{n \times r} \forall i, j$. The cubic Bézier surface is defined as:

$$\beta : [0, 1] \times [0, 1] \rightarrow \mathbb{R}^{n \times r} :$$

$$(t_1, t_2) \mapsto \beta(t_1, t_2; (b_{i,j})_{i,j=0,\dots,3}) := \sum_{i=0}^3 \sum_{j=0}^3 b_{i,j} B_{i,3}(t_1) B_{j,3}(t_2),$$

where $B_{i,3}(t) := \sum_{i=0}^3 \binom{3}{i} t^i (1-t)^{3-i}$, with $t \in [0, 1]$, is the Bernstein polynomial of order 3.

We define the patchwise cubic Bézier surface on the section, denoted φ^{BS} , as follows.

Definition 5 Assume that we have a set of data matrices $(A_{i,j})$, with $A_{i,j} \in \mathcal{S}_+(r, n)$, and with $i = 0, \dots, N_1$ and $j = 0, \dots, N_2$. Choose a section of the quotient manifold and map all the data matrices to this section to obtain $(Y_{i,j})$, with $Y_{i,j} \in \mathbb{R}_*^{n \times r}$, $i = 0, \dots, N_1$ and $j = 0, \dots, N_2$. Let $Y_{\varphi^{\text{BS}}} : [0, N_1] \times [0, N_2] \rightarrow \mathbb{R}^{n \times r}$ be the patchwise Bézier surface interpolating the data matrices $(Y_{i,j})$, and computed as in [2]. The surface φ^{BS} is obtained as follows.

$$\varphi^{\text{BS}} : [0, N_1] \times [0, N_2] \rightarrow \mathcal{S}_+(\leq r, n) : (t_1, t_2) \mapsto Y_{\varphi^{\text{BS}}}(t_1, t_2) Y_{\varphi^{\text{BS}}}(t_1, t_2)^\top. \quad (4)$$

Proposition 2 Apart from possibly a zero measure set, it holds that $\varphi^{\text{BS}} \in \mathcal{S}_+(r, n)$.

Proof: For all $(t_1, t_2) \in [0, 1] \times [0, 1]$, let $Y_{\varphi^{\text{BS}}}(t_1, t_2)$ be a representative in $\mathbb{R}_*^{n \times p}$ of $\varphi^{\text{BS}}(t_1, t_2)$. The proof is an immediate extension of Proposition 1, using the fact that $Y_{\varphi^{\text{BS}}}(t_1, t_2)$ is a polynomial function of t_1 and t_2 . \square

3.3.2 Higher-order covariance function based on the exp and log

In this case, we refer to the Bézier surface interpolation algorithm on manifolds, proposed in [2]. This algorithm relies on the expressions for the logarithm and the exponential map, provided in [41] for the manifold $\mathcal{S}_+(r, n)$. We define the surface φ^{BG} (patchwise Bézier-like on the manifold) as follows.

Definition 6 Let $(A_{i,j})$ be a data set, with $A_{i,j} \in \mathcal{S}_+(r, n)$, and with $i = 0, \dots, N_1$, $j = 0, \dots, N_2$. The surface $\varphi^{\text{BG}} : [0, N_1] \times [0, N_2] \rightarrow \mathcal{S}_+(\leq r, n)$ is the surface obtained by applying the Bézier surface interpolation algorithm on manifolds proposed in [2], with type-II reconstruction (cf. [2, Definition 4]), and with the control points chosen as suggested in [1].

Proposition 3 Under Hypothesis 1, it holds that $\varphi^{\text{BG}} \in \mathcal{S}_+(r, n)$, apart from possibly a zero measure set.

Proof: For all $(t_1, t_2) \in [0, 1] \times [0, 1]$, let $Y_{\varphi^{\text{BG}}}(t_1, t_2)$ be a representative in $\mathbb{R}_*^{n \times p}$ of $\varphi^{\text{BG}}(t_1, t_2)$. The proof is an immediate extension of Proposition 1, using the fact that $Y_{\varphi^{\text{BG}}}(t_1, t_2)$ can be written only in terms of polynomial terms in the variables t_1 and t_2 , and orthogonal factors of some real analytic matrix functions $t_1 \mapsto M(t_1)$. (This last fact is a direct consequence of the reconstruction method used: interpolation is first performed along one variable, and then along the other.) \square

3.4 Interpolation of labelled matrices using covariance functions

If the data matrices (A_i) are labelled by certain known parameters x , i.e., $A_i = A(x_i)$, it is also possible to use the covariance functions in Section 3 to perform interpolation. (In Section 5, for example, x will correspond to the magnitude and heading of the prevailing wind.)

Problem 1 (Interpolation with low-rank covariance functions) *Given matrices $A(x_i) \in \mathcal{S}_+(r, n)$ for $x_0, x_1, \dots, x_m \in \mathbb{R}^p$ and an associated low-rank covariance function, evaluate this function for any $x \in \mathbb{R}^p$.*

Of course, performing interpolation requires mapping from the label $x \in \mathbb{R}^p$ to an element of the input domain of the chosen low-rank covariance function. For example, when using the two-parameter covariance functions detailed above, constructed from $N_1 N_2$ data matrices, we need to map from a subset of \mathbb{R}^2 to $[0, N_1] \times [0, N_2]$. We will usually use affine mappings for this purpose; more details are given in Section 5, where we evaluate the interpolation capabilities of one-parameter (Section 5.2) and multi-parameter (Section 5.4.1) covariance functions.

4 Covariance identification using distance minimization

Having proposed multi-parameter low-rank covariance families in the previous section, we can now describe identification procedures within such families. That is, given a data set $(y_i)_{i=1}^q$ (assumed to be centered, with $y_i \in \mathbb{R}^n$) from which we construct a sample covariance matrix $\hat{C} = \frac{1}{q} \sum_i y_i y_i^\top$, we would like to find the most representative member of a family.

A widely used methodology for selecting a representative member of any parametric covariance family (like $\varphi_{A_1, \dots, A_m}(t)$) is maximum likelihood estimation. That is, the data are assumed to have a certain probability distribution, e.g., $Y_i \sim N(0, \varphi_{A_1, \dots, A_m}(t))$, and we choose $t \in \mathbb{R}^p$ to maximize the resulting likelihood function $p(y_1, \dots, y_q | t)$. Since $\varphi_{A_1, \dots, A_m}(t)$ are low-rank, however, the Gaussian distribution of the data is degenerate. Thus the associated probability density function is not well-defined for generic y_i and maximizing the likelihood becomes non-trivial. (If the matrices were instead SPD and as $q \rightarrow \infty$, this problem is equivalent to minimizing the Kullback–Leibler divergence of $N(0, \hat{C})$ from $N(0, \varphi_{A_1, \dots, A_m}(t))$, known as reverse information projection [20, 10, 15].)

Rather than maximizing the likelihood, we propose to minimize a particular distance from the covariance function to the sample covariance matrix \hat{C} .

Problem 2 (Minimum Frobenius distance covariance identification)

$$\arg \min_{t \in \mathbb{R}^p} d_F(\varphi_{A_1, \dots, A_m}(t), \hat{C}),$$

where $d_F(A_1, A_2) = \|A_1 - A_2\|_F$ is the Frobenius distance.

This is a particular instance of “minimum distance estimation”; such estimators, in general, have a long history in statistics [61].

We now discuss solutions to Problem 2 given particular constructions of the covariance function $\varphi(t)$. Since the geodesic and sectional approaches to define covariance functions coincide for the one-parameter case under some conditions (cf. Remark 1), we divide this section in two parts: the one-parameter case ($p = 1$) and the multi-parameter case. For the latter, we focus on the case of two parameters ($p = 2$).

4.1 One-parameter first-order covariance function

For $p = 1$, the covariance function $t_1 \mapsto \varphi(t_1)$ is simply the geodesic between the two data matrices. The optimization problem has a closed form solution that is presented below.

Proposition 4 (Solution of the low-rank covariance identification problem) *The solutions of Problem 2 for $p = 1$ are the roots of a third order polynomial $at^3 + bt^2 + ct + d = 0$ with:*

$$\begin{aligned} a &= 4 \operatorname{tr}(\dot{Y}_{A_1 \rightarrow A_2} \dot{Y}_{A_1 \rightarrow A_2}^\top \dot{Y}_{A_1 \rightarrow A_2} \dot{Y}_{A_1 \rightarrow A_2}^\top), \\ b &= 12 \operatorname{tr}(Y_{A_1} \dot{Y}_{A_1 \rightarrow A_2}^\top \dot{Y}_{A_1 \rightarrow A_2} Y_{A_1} \dot{Y}_{A_1 \rightarrow A_2}^\top), \\ c &= 4 \operatorname{tr}(2Y_{A_1} Y_{A_1}^\top \dot{Y}_{A_1 \rightarrow A_2} \dot{Y}_{A_1 \rightarrow A_2}^\top + Y_{A_1} \dot{Y}_{A_1 \rightarrow A_2}^\top Y_{A_1} \dot{Y}_{A_1 \rightarrow A_2} - \dot{Y}_{A_1 \rightarrow A_2} \dot{Y}_{A_1 \rightarrow A_2}^\top Y_{\hat{C}} Y_{\hat{C}}^\top), \\ d &= 4 \operatorname{tr}(Y_{A_1} Y_{A_1}^\top \dot{Y}_{A_1 \rightarrow A_2} Y_{A_1}^\top - \dot{Y}_{A_1 \rightarrow A_2} Y_{A_1}^\top Y_{\hat{C}} Y_{\hat{C}}^\top). \end{aligned}$$

Proof: The cost function is:

$$d_F(\varphi_{A_1 \rightarrow A_2}(t), \hat{C}) = \sqrt{\operatorname{tr}((\varphi_{A_1 \rightarrow A_2}(t) - \hat{C})(\varphi_{A_1 \rightarrow A_2}(t) - \hat{C})^\top)}.$$

The third-order polynomial is obtained after setting the derivative to zero and noting that the optimization problem is unconstrained. \square

Proposition 4 provides at least one solution. If there are three roots, the minimizer is of course the one with smallest objective. As with any third order polynomial, the uniqueness condition of this solution is:

$$18abcd - 4b^3d + b^2c^2 - 4ac^3 - 27a^2d^2 \leq 0.$$

The computational cost of finding the solution of the low-rank covariance identification problem is only $\mathcal{O}(nr)$. Indeed, roots of the cubic equation have a closed form expression whose evaluation does not require any meaningful cost. The only computational cost is that associated with computing traces to obtain the polynomial coefficients. By virtue of the cyclic property of the trace, we can compute these traces with $\mathcal{O}(nr)$ elementary operations.

4.2 Two-parameter first-order covariance functions

Here we focus on Problem 2 in the two-parameter case ($p = 2$) for first-order covariance functions, i.e., $\varphi = \varphi^{\text{LS}}$ or $\varphi = \varphi^{\text{LG}}$ (cf. Definition 4). Similarly to the previous sections, we assume that data matrices are defined on a grid of points $(A_{i,j})$, with $A_{i,j} \in \mathcal{S}_+(r, n)$, $i = 0, \dots, N_1$ and $j = 0, \dots, N_2$.

4.2.1 First-order sectional covariance function

In the case $\varphi = \varphi^{\text{LS}}$ (see Definition 4), we propose to use a gradient descent on each patch of the surface. Observe indeed that the surface φ^{LS} is generally nondifferentiable (actually, even noncontinuous) on the borders of the patches. The global optimum is then computed as the minimum of the optima obtained on the patches. Let

$$f : [0, N_1] \times [0, N_2] \rightarrow \mathbb{R} : (t_1, t_2) \mapsto f(t_1, t_2) := d_F(\varphi^{\text{LS}}(t_1, t_2), \hat{C})^2 \quad (5)$$

be the cost function to minimize.

Consider an arbitrary patch (l, m) , with $l = 0, \dots, N_1 - 1$ and $m = 0, \dots, N_2 - 1$. Let $f^{l,m}$ be the restriction of f to the patch (l, m) , and let $A_{l,m}$, $A_{l+1,m}$, $A_{l,m+1}$, $A_{l+1,m+1}$ denote the four

corners of the patch (l, m) , and $\bar{Y}_{A_{l,m}}, \bar{Y}_{A_{l+1,m}}, \bar{Y}_{A_{l,m+1}}, \bar{Y}_{A_{l+1,m+1}}$ their projection on the section. We omit the superscript LS in the remainder of this section. The gradient of the restriction of the cost function (5) to that patch can be computed explicitly:

$$\frac{\partial f^{l,m}}{\partial t_1}(t_1, t_2) = 2 \operatorname{tr} D\varphi(t_1, t_2)[e_1](\varphi(t_1, t_2) - \hat{C})^\top, \quad (6)$$

$$\frac{\partial f^{l,m}}{\partial t_2}(t_1, t_2) = 2 \operatorname{tr} D\varphi(t_1, t_2)[e_2](\varphi(t_1, t_2) - \hat{C})^\top, \quad (7)$$

with $D\varphi(t_1, t_2)[e_1]$ and $D\varphi(t_1, t_2)[e_2]$ defined as:

$$\begin{aligned} D\varphi(t_1, t_2)[e_1] &= DY_\varphi(t_1, t_2)[e_1]Y_\varphi^\top + Y_\varphi DY_\varphi(t_1, t_2)[e_1]^\top, \\ D\varphi(t_1, t_2)[e_2] &= DY_\varphi(t_1, t_2)[e_2]Y_\varphi^\top + Y_\varphi DY_\varphi(t_1, t_2)[e_2]^\top. \end{aligned}$$

The factor Y_φ was defined in Definition 2:

$$Y_\varphi = \bar{Y}_{A_{l,m}}(1-t_1)(1-t_2) + \bar{Y}_{A_{l+1,m}}(1-t_1)t_2 + \bar{Y}_{A_{l,m+1}}t_1(1-t_2) + \bar{Y}_{A_{l+1,m+1}}t_1t_2.$$

So $DY_\varphi(t_1, t_2)[e_1]$ and $DY_\varphi(t_1, t_2)[e_2]$ can be easily obtained as:

$$\begin{aligned} DY_\varphi(t_1, t_2)[e_1] &= t_2(\bar{Y}_{A_{l,m}} - \bar{Y}_{A_{l+1,m}} - \bar{Y}_{A_{l,m+1}} + \bar{Y}_{A_{l+1,m+1}}) + \bar{Y}_{A_{l,m+1}} - \bar{Y}_{A_{l,m}}, \\ DY_\varphi(t_1, t_2)[e_2] &= t_1(\bar{Y}_{A_{l,m}} - \bar{Y}_{A_{l+1,m}} - \bar{Y}_{A_{l,m+1}} + \bar{Y}_{A_{l+1,m+1}}) + \bar{Y}_{A_{l+1,m}} - \bar{Y}_{A_{l,m}}, \end{aligned}$$

with the only difference being the parameter t_1 vs. t_2 .

4.2.2 First-order geodesic covariance function

We focus now on Problem 2 for $p = 2$, when the covariance function is the surface φ^{LG} defined in Definition 4. Let

$$f : [0, N_1] \times [0, N_2] \rightarrow \mathbb{R} : (t_1, t_2) \mapsto f(t_1, t_2) := d_F(\varphi^{\text{LG}}(t_1, t_2), \hat{C})^2 \quad (8)$$

be the cost function. The surface φ^{LG} is generally not differentiable on the borders of the patches. As a result, similarly to the previous section, we propose to run an optimization algorithm to find the optimum on each patch, and to compare the optimal values obtained on the patches to obtain the global optimum.

Let $f^{l,m}$ be the restriction of f to the patch (l, m) . We propose to minimize $f^{l,m}$ by expressing it as a one-variable function, replacing t_2 by its optimal value:

$$t_2^*(t_1) = \operatorname{argmin}_{t_2 \in \mathbb{R}} f^{l,m}(t_1, t_2), \quad (9)$$

and then to apply gradient descent to the problem:

$$\min_{t_1 \in \mathbb{R}} \tilde{f}^{l,m}(t_1) := f^{l,m}(t_1, t_2^*(t_1)). \quad (10)$$

The computation of the partial derivatives required by both steps is deferred to Appendix A.

4.3 Higher-order covariance functions using Bézier curves

We now solve Problem 2 for $p = 2$ when the surface is defined from Bézier interpolating surfaces.

4.3.1 Higher-order sectional covariance function

To solve Problem 2 for $p = 2$ when the surface is a Euclidean Bézier surface built in a given section of the manifold, we propose again to use steepest descent. The cost function

$$f : [0, N_1] \times [0, N_2] \rightarrow \mathbb{R} : (t_1, t_2) \mapsto f(t_1, t_2) := d_F(\varphi^{\text{BS}}(t_1, t_2), \hat{C})^2, \quad (11)$$

with φ^{BS} defined in Definition 5, is \mathcal{C}^1 . Moreover, since Bézier curves in the Euclidean space are weighted sums of Bernstein polynomials, the gradient can be computed explicitly. The computation of the gradient is similar to Section 4.2.1, except that now Y_φ is obtained as a linear combination of cubic Bernstein polynomials:

$$Y_\varphi(t_1, t_2) = \sum_{i=0}^3 \sum_{j=0}^3 b_{ij} B_{i3}(t_1) B_{j3}(t_2).$$

The derivatives $DY_\varphi(t_1, t_2)[e_1]$ and $DY_\varphi(t_1, t_2)[e_2]$ become:

$$\begin{aligned} DY_\varphi(t_1, t_2)[e_1] &= \sum_{i=0}^3 \sum_{j=0}^3 b_{ij} \dot{B}_{i3}(t_1) B_{j3}(t_2), \\ DY_\varphi(t_1, t_2)[e_2] &= \sum_{i=0}^3 \sum_{j=0}^3 b_{ij} B_{i3}(t_1) \dot{B}_{j3}(t_2). \end{aligned}$$

4.3.2 Higher-order covariance function based on the exponential and logarithm maps

For φ^{BG} in Definition 6, it remains unclear whether the gradient of the cost function:

$$f : [0, N_1] \times [0, N_2] \rightarrow \mathbb{R} : (t_1, t_2) \mapsto d_F(\varphi^{\text{BG}}(t_1, t_2), \hat{C})^2. \quad (12)$$

has an analytical expression. Variable projection methods also do not seem applicable in this case. Thus we have to estimate the gradient numerically, resorting to finite differences.

5 Case study: wind field approximation

Given the increasing popularity of unmanned aerial vehicles (UAVs) in transportation, surveillance, agriculture, and beyond, accurate and safe aerial navigation is essential. Achieving these requirements demands expressive models of the UAV's environment—in particular, the wind field—and the ability to update these models given new observations, e.g., via Kalman filtering [49, 16]. To this end, we wish to construct and estimate the covariance of spatially distributed wind velocity components.

5.1 Model problem and data set

Gaussian random field (GRF) models have previously been used to describe wind velocities (e.g., [62, 33]). A common practice in this setting is to define the covariance matrix of the velocities using the (smooth) squared-exponential kernel, perhaps with some modifications to allow for non-stationarity [34]. We instead assume to have instances of the covariance matrix for different values of the prevailing wind heading θ and magnitude W ; from these instances, we will build a covariance family for continuous (θ, W) . The wind field can change dramatically as function of

the prevailing wind, and thus it is useful to consider a covariance family built from a variety of representative prevailing wind settings.

In general, these instances could be estimated from observational data, or they could be constructed using offline (and potentially expensive) computational fluid dynamics simulations. Here we use the latter: we solve the unsteady incompressible Navier–Stokes equations on the two-dimensional domain shown in Figure 4, using direct numerical simulation with a spectral element method. The Reynolds number in our simulations, defined according to the side-length of the central obstacle, is around 500 for $W = 7.0$. For each chosen value of (θ, W) , we run the simulation until any transients due to the initial condition have dissipated and then collect instantaneous velocity fields as “snapshots,” shown in Figure 4. The sample covariance of these snapshots provides the data covariance matrix at that (θ, W) .

The right plot of Figure 3 represents a notional idea of our example domain: flow around a rectangular cuboid in three dimensions. We consider only a horizontal “slice” of this domain, e.g., the wind in a plane at height h sufficiently far from the ground and from top of the obstacle so that a two-dimensional approximation is reasonable. The left plot of Figure 3 shows the mean value of the velocity on this plane, at an example value of (θ, W) . The grid size is 39×39 , and hence the discretized wind field has $n = 3024 = 2 \times (39^2 - 9)$ degrees of freedom: two velocity components at each grid point, subtracting 9 points for the obstacle. The grey contours represent the pointwise variance of the x -velocity plus that of the y -velocity (i.e., the sum of two diagonal entries of the covariance matrix, at each point in space). Naturally, the variance is larger downstream of the obstacle, where vortices are shed.

Our data set for the examples below comprises a set of covariance matrices $C(\theta_k, W_i)$, with $\theta_k = (k - 1)\pi/64$, $k \in 1, \dots, 32$ and $W \in \{4.0, 5.5, 7.0, 8.5, 10.0, 11.5, 13.0\}$, as illustrated in Figure 8. Using a truncated singular value decomposition of each matrix, we reduce the rank to $r = 20$. These covariance matrices then belong to $\mathcal{S}_+(20, 3024)$.

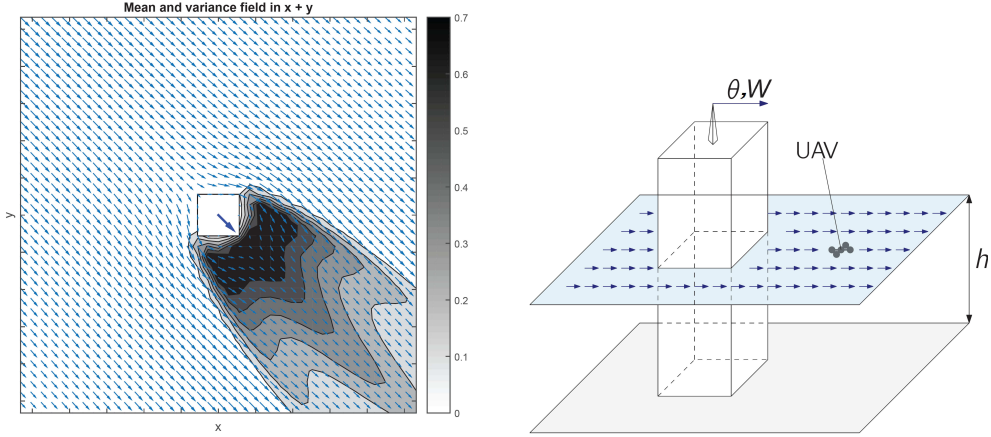


Figure 3: Representation of the wind field. Left: two-dimensional domain, with wind field around the square obstacle represented by light blue arrows and the prevailing wind in dark blue; gray contours are the variance field. Right: notional 3-D problem, with a section of the wind field at an altitude h .

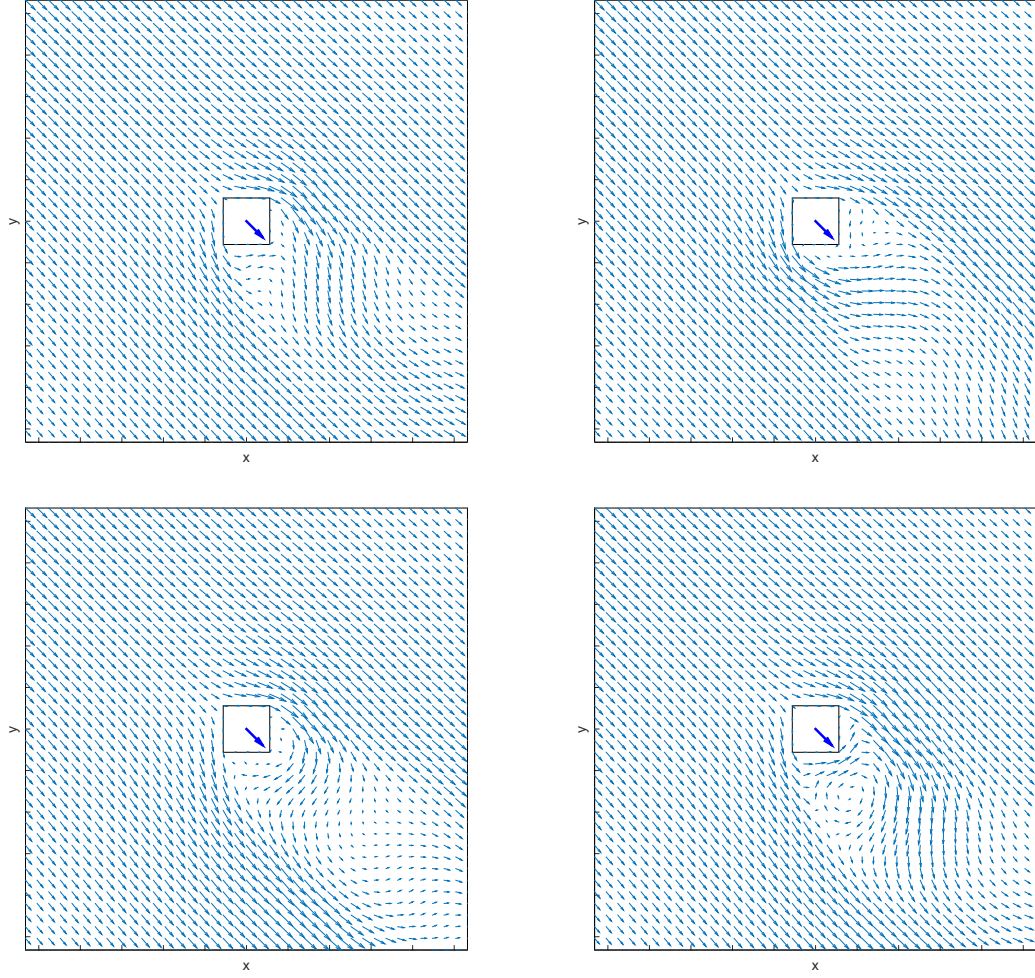


Figure 4: Instantaneous snapshots of the wind velocity field for $\theta = 45$ and $W = 7$.

5.2 One-parameter covariance families

We first consider interpolation and identification with a one-parameter geodesic covariance function $\varphi_{A_1 \rightarrow A_2}(t)$, where the data matrices A_1 and A_2 are obtained at the same wind magnitude but at faraway headings: $A_1 = C(\theta_1 = 0, W = 8.5)$ and $A_2 = C(\theta_9 = 23, W = 8.5)$. (As noted in Remark 1, the one-parameter geodesic and sectional families coincide.) To understand the relationship between the geodesic parameter t and the true wind heading, we minimize the distance from each of the seven intermediate data matrices $C(\theta_k, 8.5)$, $k \in 1, 2, \dots, 9$, to this covariance family (cf. red line in Figure 8) and obtain a value of t_k . Figure 5 shows the resulting pairs (θ_k, t_k) . The relationship between t and θ is monotone and nearly linear. Similar results can be obtained for other choices of W .

Next we focus on the shape of the objective function used in distance minimization for one-dimensional covariance families. We build a one-parameter covariance function $\varphi_{A_1 \rightarrow A_2}(t)$ with $A_1 = C(16.9, 7)$ and $A_2 = C(22.5, 7)$ and evaluate the distance to $A_3 = C(19.7, 7)$ as a function of

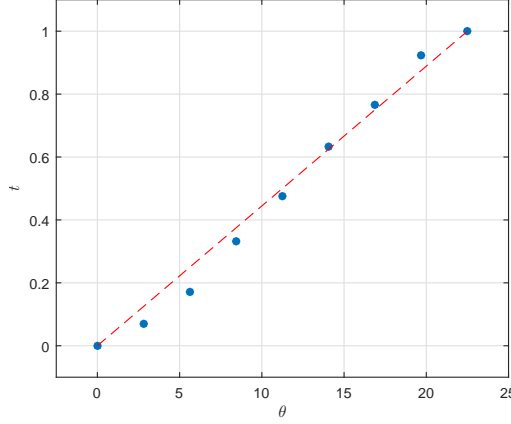


Figure 5: Minimizing value of t (blue points) for data drawn from a range of wind headings θ , for $W = 8.5$ (cf. Section 5.2). The red line represents a “perfect” linear relationship.

$t \in [0, 1]$. (See Figure 8, dashed blue line, to identify the relevant matrices in our data set.) This exercise is shown in Figure 6, where the anchor or data matrices A_1, A_2 are illustrated via inset plots with a green obstacle. (The matrices are visualized by their variance fields, as in Figure 3 (left).) First, we note that the distance objective is smooth and convex (on $[0, 1]$), and that its minimum (marked with a blue dot) is close to, though not exactly, $t = 0.5$. This offset is a further instance of the difference illustrated in Figure 5, between the minimum-distance points and a perfect linear relationship. The inset plots in Figure 6 with white obstacles show covariances in the one-dimensional family at intermediate values of t ; we see that these covariances look physically reasonable, suggesting intermediate wind headings as desired. Nonetheless, we also note that the minimum Frobenius distance from A_3 to this family is roughly 14, about half of the distance from A_3 to the anchor A_1 . For a more accurate representation of A_3 , one may thus want a richer family or more representative data matrices. We will explore these choices below.

5.3 Distances to two-parameter covariance families

Now we illustrate the distance between a given matrix and two different two-parameter covariance families, each constructed from the same four data matrices. The minimizer of this distance is a solution of Problem 2.

First, we consider the first-order sectional covariance function of Section 3.1. We use four data matrices: $A_1 = C(11.3, 4)$, $A_2 = C(11.3, 10)$, $A_3 = C(16.9, 4)$, $A_4 = C(16.9, 10)$. Figure 7 (left) illustrates the distance from $\varphi^{\text{LS}}_{(A_1 \rightarrow A_2) \rightarrow (A_3 \rightarrow A_4)}(t_1, t_2)$ to $A_5 = C(14.1, 7)$. The red triangle represents distance minimizer, which lies at $t_1 = 0.48$ and $t_2 = 0.77$ and yields a distance of 5.5 from the target. To define the section in this case, we use the matrix A_1 . The four anchor matrices are the edges of the rectangle in Figure 8; other choices would lead to similar results, as analyzed in subsequent subsections.

Next, we repeat the study for the geodesic two-parameter covariance function defined in Section 3.1.2, with results shown in Figure 7 (right). Again, the minimizer is marked with a red triangle, which lies at $t_1 = 0.77$ and $t_2 = 0.48$ and yields a distance of 5.5 from the target. Note that the inputs to both covariance functions can in principle be any element of \mathbb{R}^2 ; here, both figures show the distance for $(t_1, t_2) \in [0, 2] \times [-1, 1]$. The distance contours are shaped slightly differently for the sectional and geodesic cases, though the minimizer lies in the top left quadrant

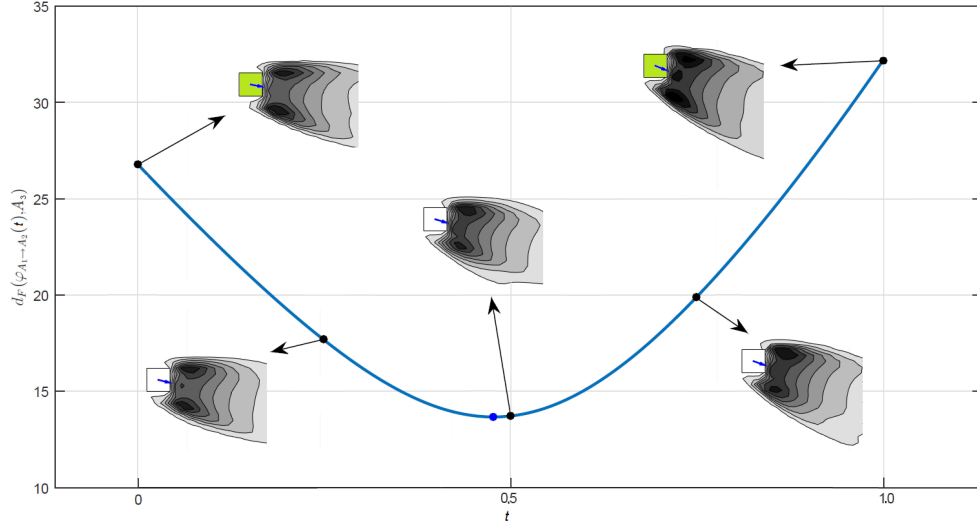


Figure 6: Distance from $A_3 = C(19.7, 7)$ to the one-parameter covariance family built from $A_1 = C(16.9, 7)$ and $A_2 = C(22.5, 7)$, as a function of the input variable t . A_1 and A_2 are marked with green obstacles to identify them as the data matrices/anchors. The blue point represents the distance minimizer.

$[0, 1]^2$ of each figure, as expected.

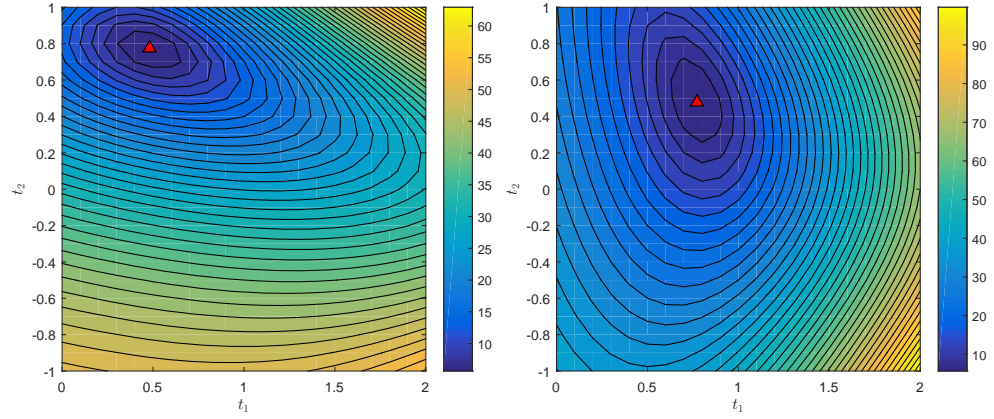


Figure 7: Left: Distance from A_5 to $\varphi^{\text{LS}}_{(A_1 \rightarrow A_2) \rightarrow (A_3 \rightarrow A_4)}(t_1, t_2)$. Right: Distance from A_5 to $\varphi^{\text{LG}}_{(A_1 \rightarrow A_2) \rightarrow (A_3 \rightarrow A_4)}(t_1, t_2)$.

5.4 Benchmarking first-order and higher-order covariance functions

Now we consider the four surfaces defined in Section 3: the first-order covariance functions φ^{LS} and φ^{LG} defined patchwise (see Definition 4), and the Bézier-like covariance functions φ^{BS} and φ^{BG} (see Definitions 5 and 6).

For the surfaces defined on a section of the manifold, we consider several possibilities: for

φ^{LS} , the section based at one of the data matrices (here, the lower left data matrix of the patch), based at the arithmetic mean of the data matrices, or based at the inductive mean of the four data matrices of the patch. For φ^{BS} , the section is based at one of the data matrices (here, the lower left data matrix of the training set), at the arithmetic mean of the data matrices of the training set, or at the inductive mean of the four data matrices of the training set.

These combinations lead to a total of eight surfaces. The data matrices are split into two sets shown in Figure 8: the blue points and the black points. The blue points are used to construct the surface, and the accuracy of the methods is evaluated on the black points.

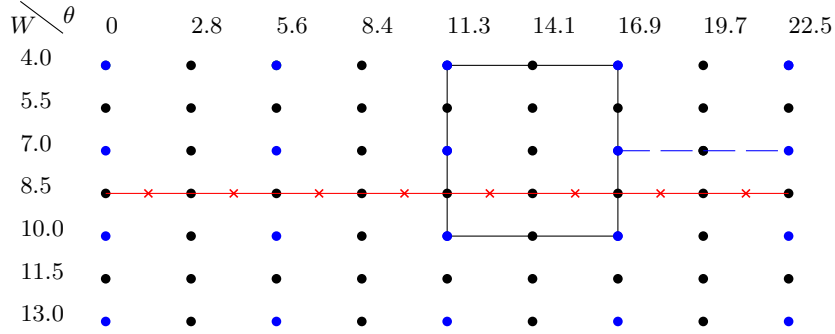


Figure 8: Data set for the wind field problem; each dot shows the wind magnitude W and heading θ corresponding to a data covariance matrix. The red (crossed) and blue (dashed) lines represent the data used in Section 5.2. The rectangle illustrates the operating zone of Section 5.3. The blue nodes comprise the training set and the black nodes the test set for Sections 5.4.1 and 5.4.2.

5.4.1 Interpolation errors

The error

$$E(C(\theta, W)) := \|C(\theta, W) - \varphi^{\text{method}}(\theta, W)\|_F^2$$

is a measure of the ability of the surface φ^{method} to recover some hidden covariance matrix $C(\theta, W)$.¹ We will also consider the normalized error

$$E_N(C(\theta, W)) := 100 \times \frac{\|C(\theta, W) - \varphi^{\text{method}}(\theta, W)\|_F^2}{\frac{1}{4} \sum_{j=1}^4 \|C(\theta, W) - A_j\|_F^2},$$

where normalization is performed with respect to the average squared distance between the target matrix $C(\theta, W)$ and the four corners of the patch to which it belongs, according to the grid representation in Figure 8. (The patch is chosen systematically as the one below and to the left of the test point considered.)

Having defined these interpolation errors for arbitrary $C(\theta, W)$, we now evaluate them for all the points $C(\theta_i, W_i)$ in the test set—i.e., for each of the data matrices marked with black nodes in Figure 8. We average the errors over the test set and report the resulting values in Table 1.

Some takeaways from this study are as follows. First, the matrix chosen to define the section in either the first-order sectional covariance function or the higher-order sectional covariance

¹Here we write φ^{method} with arguments (θ, W) in a slight abuse of notation. More precisely, we mean that the two-parameter covariance function φ^{method} is evaluated at (t_1, t_2) corresponding to an affine mapping from the range of (θ, W) (here $[0, 22.5] \times [4, 13]$) to $[0, 4] \times [0, 3]$, consistent with the 5×4 grid of data matrices.

	$\text{avg}_i [E(C(\theta_i, W_i))]$	$\text{avg}_i [E_N(C(\theta_i, W_i))]$
1st-order section $\varphi_{\text{one}}^{\text{LS}}$	30.3	7.78
1st-order section $\varphi_{\text{arithm}}^{\text{LS}}$	30.4	7.80
1st-order section $\varphi_{\text{inductive}}^{\text{LS}}$	30.3	7.77
1st-order geodesic φ^{LG}	30.3	7.77
Bézier section $\varphi_{\text{one}}^{\text{BS}}$	20.8	4.91
Bézier section $\varphi_{\text{arithm}}^{\text{BS}}$	20.5	4.87
Bézier section $\varphi_{\text{inductive}}^{\text{BS}}$	20.4	4.85
Bézier geodesic φ^{BG}	20.3	4.79

Table 1: Average (squared) distance separating a given test point $C(\theta_i, W_i)$ from the corresponding interpolation point on the different surfaces. For the methods defined on a section of the manifold, the subscript of φ indicates how the section was chosen: ‘one’ means that we use one of the data matrices (here, the matrix at the lower left corner of the patch) as basis of the section, while ‘arithm’ and ‘inductive’ denote, respectively, the arithmetic and inductive means of the corners of the patch.

function seems to have little impact. Moreover, the performance of the geodesic covariance functions is not noticeably better than that of the sectional functions in this setting. But the interpolation performance of the higher-order (Bézier) families is significantly better than that of the first-order families.

5.4.2 Identification errors and data compression

We now assess identification errors within the covariance families. In other words, we now use the techniques of Section 4 to minimize the distance from each element of the test set to the covariance family φ^{method} , built patchwise from the training matrices. From another perspective, this process can be viewed as data compression: a simple way to perform data compression consists of storing only several matrices (in our case, the training data) and then storing, for any additional matrix, the coordinates of the closest point in the surface. We now compare our surfaces for this task. Similarly to the previous section, we use the following two error measures,

$$E^*(C(\theta_i, W_i)) = \|C(\theta_i, W_i) - \varphi(t_1^*(i), t_2^*(i))\|_F^2,$$

$$E_N^*(C(\theta_i, W_i)) = \frac{100 \times \|C(\theta_i, W_i) - \varphi(t_1^*(i), t_2^*(i))\|_F^2}{\frac{1}{4} \sum_{j=1}^4 \|C(\theta_i, W_i) - A_j\|_F^2},$$

where A_j are the four corners of the patch to which $C(\theta_i, W_i)$ belongs and $t_1^*(i), t_2^*(i)$ are the solutions to the optimization problem discussed in Section 4.

We evaluate these errors for every test matrix and report, in Table 2, the average errors for each surface definition proposed. These are essentially the average distance between an element of our test set and the closest point on the surface. A key takeaway from this table is that the error are significantly lower than those in Table 1; this is not surprising, as here we are optimizing to find the best point in each family. Also, results with the geodesic families in this example appear to be slightly better than with the sectional families.

It is instructive to see how the normalized errors $E_N^*(C(\theta_i, W_i))$ are distributed over the data set, i.e., how the approximation error depends on the parameters of the data matrices $C(\theta_i, W_i)$. We illustrate this distribution using the stem plot in Figure 9, for φ^{BG} only. Errors are largest for wind field headings between those of the training set (i.e., $\theta \in \{2.8, 8.4, 14.1, 19.7\}$) and increase strongly with the wind field magnitude. These trends indicate that it might be useful to generate

	$\text{avg}_i [E^*(C(\theta_i, W_i))]$	$\text{avg}_i [E_N^*(C(\theta_i, W_i))]$
1st-order section $\varphi_{\text{one}}^{\text{LS}}$	21.8	5.30
1st-order section $\varphi_{\text{arithm}}^{\text{LS}}$	21.8	5.29
1st-order section $\varphi_{\text{inductive}}^{\text{LS}}$	21.8	5.30
1st-order geodesic φ^{LG}	20.9	5.10
Bézier section $\varphi_{\text{one}}^{\text{BS}}$	14.3	3.34
Bézier section $\varphi_{\text{arithm}}^{\text{BS}}$	14.0	3.29
Bézier section $\varphi_{\text{inductive}}^{\text{BS}}$	14.0	3.29
Bézier geodesic φ^{BG}	13.8	3.24

Table 2: Average (squared) distance separating a given test point from its closest approximation on the different surfaces. For methods defined on a section of the manifold, the subscript of φ indicates how the section was chosen: ‘one’ means that we use one of the data matrices (here, the matrix at the lower left corner of the patch) as basis of the section, while ‘arithm’ and ‘inductive’ denote, respectively, the arithmetic and inductive means of the corners of the patch.

a denser grid of data matrices in the θ direction, particularly for large W , and to use a coarser grid in the W direction.

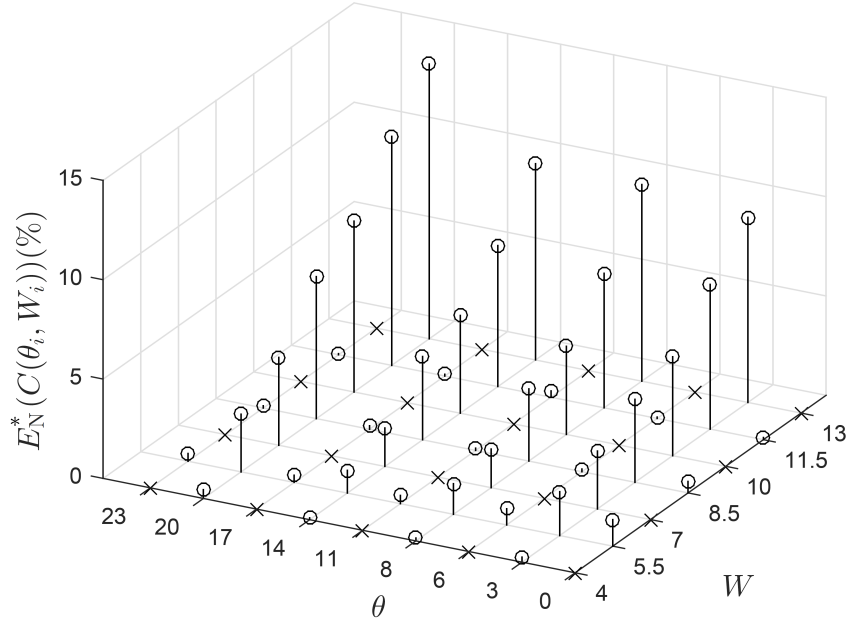


Figure 9: Distribution of the errors obtained with the higher-order geodesic covariance family φ^{BG} . Crosses are training points, circles are test points. It is more difficult to recover the data when varying θ , particularly at larger W . Interpolation in the W direction, on the other hand, yields very small errors.

6 Conclusions

We have presented a differential geometric framework for constructing parametric low-rank covariance families, by connecting low-rank covariance matrices obtained at representative problem instances. In this sense, our framework creates parametric covariance families that can easily incorporate prior knowledge or empirical information, via the given data matrices or anchors. Within this broad framework, we have proposed several different constructions that rely on geodesics on the manifold of positive-semidefinite matrices, or on affine sections of this manifold. We presented particular instances of such covariance functions that interpolate grids of data matrices, using either first- or higher-order (Bézier) approaches.

Given some data and the resulting sample covariance matrix (which can be strongly rank-deficient) we show how to perform minimum-distance covariance identification, that is, how to find the closest element of a given covariance family. We discuss methods and algorithms to solve this problem for each of the proposed covariance functions. In a case study involving wind velocity field approximation, we assess the ability of our covariance families to represent out-of-family covariance matrices. We also demonstrate the possibility of using this technique for data compression, i.e., storing the parameters of the family corresponding to a particular matrix, instead of the matrix itself.

Moreover, if the data matrices are labelled by some characteristics of the problem, we observe that our covariance functions achieve a natural or desirable behavior—in that the inputs to these functions (related to distance along a geodesic or a sectional projection) are closely related to the label parameters themselves. For instance, our case study shows that a family constructed from covariance matrices obtained at very different wind headings contains matrices that match all intermediate headings, and that the input parameter to the covariance function and the wind heading can be nearly linearly related.

An advantage of the proposed framework is that one can choose the rank of the resulting matrices. To illustrate, in the case study, although the dimension of the covariance matrices is high ($n = 3024$), we can reduce the rank to $r = 20$, saving considerable computational cost while still obtaining good approximations.

We also note that this paper has focused on the definition and construction of low-rank covariance families, and on efficient optimization methods for solving identification problems within these families. An interesting and complementary line of work could analyze certain associated statistical questions, i.e., statistical properties of the minimum distance estimator as a function of the sample size q , the matrix dimension n , and the chosen rank r . We defer such investigations to future work.

Implementation code

The code to generate covariance functions and to perform identification and interpolation is available at https://github.com/EMassart/covariance_fitting.

A Computation of the tools required for the variable projection method

We detail here the computations for the main steps of the variable projection method proposed in Section 4.2.2. Remember that the corresponding surface, $\varphi^{\text{LG}}(t_1, t_2) = Y_\varphi(t_1, t_2)Y_\varphi(t_1, t_2)^\top$,

where Y_φ is obtained by composition of two geodesics, respectively along the t_1 and t_2 variables:

$$\begin{aligned} Y_\varphi(t_1, t_2) &:= (1 - t_2)Y_{1-2}(t_1) + t_2Y_{3-4}(t_1)Q(t_1)^\top, \\ Y_{1-2}(t_1) &:= (1 - t_1)Y_1 + t_1Y_2Q_{1-2}^\top, \\ Y_{3-4}(t_1) &:= (1 - t_1)Y_3 + t_1Y_4Q_{3-4}^\top. \end{aligned}$$

A.1 Computation of the partial derivative with respect to t_1

Computing the partial derivative of the function $(t_1, t_2) \mapsto \varphi^{\text{LG}}(t_1, t_2)$ with respect to t_1 yields:

$$D\varphi^{\text{LG}}(t_1, t_2)[e_1] = DY_\varphi(t_1, t_2)[e_1] Y_\varphi(t_1, t_2)^\top + Y_\varphi(t_1, t_2) DY_\varphi(t_1, t_2)[e_1]^\top,$$

with

$$DY_\varphi(t_1, t_2)[e_1] = (1 - t_2)\dot{Y}_{1-2}(t_1) + t_2\dot{Y}_{3-4}(t_1)Q(t_1)^\top + t_2Y_{3-4}(t_1)\dot{Q}(t_1)^\top.$$

The values of $\dot{Y}_{1-2}(t_1)$ and $\dot{Y}_{3-4}(t_1)$ are independent of t_1 :

$$\dot{Y}_{1-2}(t_1) = -Y_1 + Y_2Q_{1-2}^\top, \quad \dot{Y}_{3-4}(t_1) = -Y_3 + Y_4Q_{3-4}^\top, \quad \forall t_1.$$

The value of $\dot{Q}(t_1)$ can be obtained as follows. Recall from the geodesic definition that $Q(t_1)$ is the orthogonal factor of the polar decomposition of the matrix $M(t_1) = Y_{1-2}(t_1)^\top Y_{3-4}(t_1)$, which means that there exists a symmetric positive definite matrix $H(t_1)$ such that $M(t_1) = H(t_1)Q(t_1)$. Then,

$$\dot{M}(t_1) = \dot{H}(t_1)Q(t_1) + H(t_1)\dot{Q}(t_1), \quad (13)$$

where $\dot{H}(t_1)$ is a symmetric matrix, and $\dot{Q}(t_1)$ is of the form $\dot{Q}(t_1) = \Omega(t_1)Q(t_1)$, with $\Omega(t_1)$ a skew-symmetric matrix. Right-multiplying this expression by $Q(t_1)^\top$ yields:

$$\dot{M}(t_1)Q(t_1)^\top = \dot{H}(t_1) + H(t_1)\Omega(t_1), \quad (14)$$

while left-multiplying the transpose of equation (13) by $-Q(t_1)$ yields:

$$-Q(t_1)\dot{M}(t_1)^\top = -\dot{H}(t_1) + \Omega(t_1)H(t_1). \quad (15)$$

Now, summing equations (14) and (15) yields:

$$\dot{M}(t_1)Q(t_1)^\top - Q(t_1)\dot{M}(t_1)^\top = H(t_1)\Omega(t_1) + \Omega(t_1)H(t_1).$$

As a result, the term $\dot{Q}(t_1)$ can be obtained by solving a Sylvester equation. Moreover, since $H(t_1)$ is always positive definite (except in the set of zero measure corresponding to low-rank matrices $Y_{1-2}(t_1)^\top Y_{3-4}(t_1)$), the solution to the Sylvester equation is unique ($H(t_1)$ and $-H(t_1)$ have no common eigenvalues).

A.2 Computation of $t_2^*(t_1)$

The first-order optimality condition

$$\left. \frac{\partial f}{\partial t_2} \right|_{(t_1, t_2^*(t_1))} = 0$$

implies that the optimal value $t_2^*(t_1)$ corresponding to an arbitrary value t_1 is the solution to a cubic equation:

$$s_1(t_1)t_2^3(t_1) + s_2(t_1)t_2^2(t_1) + s_3(t_1)t_2(t_1) + s_4(t_1) = 0, \quad (16)$$

with

$$\begin{aligned}
s_1(t_1) &= 2 \operatorname{tr} R^2 = 2 \sum_i \sum_j R_{ij}^2, \\
s_2(t_1) &= 3 \operatorname{tr} RS = 3 \sum_i \sum_j R_{ij} S_{ij}, \\
s_3(t_1) &= 2 \operatorname{tr} RT + \operatorname{tr} S = 2 \sum_i \sum_j R_{ij} T_{ij} + S_{ij}^2, \\
s_4(t_1) &= 2 \operatorname{tr} ST = 2 \sum_i \sum_j S_{ij} T_{ij}.
\end{aligned}$$

The matrices R , S , and T arising in those expressions are defined as:

$$\begin{aligned}
R &= Y_{1-2} Y_{1-2}^\top + Y_{3-4} Y_{3-4}^\top - (Y_{1-2} Q Y_{3-4}^\top + Y_{3-4} Q^\top Y_{1-2}^\top), \\
S &= (Y_{1-2} Q Y_{3-4}^\top + Y_{3-4} Q^\top Y_{1-2}^\top) - 2 Y_{1-2} Y_{1-2}^\top, \\
T &= Y_{1-2} Y_{1-2}^\top - \widehat{C},
\end{aligned}$$

with all these matrices depending on t_1 . Observe, however, that for a fixed value of t_1 , the function $t_2 \rightarrow f(t_1, t_2)$ might not be convex; hence, the condition (16) might have several (up to three) real solutions. In that case, we compute the value of the cost function at those solutions, and we choose the one corresponding to the smallest value of f .

A.3 Gradient descent for the univariate cost function

We are now looking for the derivative of the cost function $\tilde{f}(t_1) = f(t_1, t_2^*(t_1))$, with respect to the variable t_1 , in order to be able to apply a steepest descent method to that problem. Using the notation $\tilde{f} = F \circ \tilde{\varphi}^{\text{LG}}$, with $\tilde{\varphi}^{\text{LG}}(t_1) = \varphi^{\text{LG}}(t_1, t_2^*(t_1))$, we have:

$$\dot{\tilde{f}}(t_1) = DF[\dot{\tilde{\varphi}}^{\text{LG}}(t_1)] = 2 \operatorname{tr} \dot{\tilde{\varphi}}^{\text{LG}}(t_1) (\tilde{\varphi}^{\text{LG}}(t_1) - \widehat{C})^\top.$$

The derivative $\dot{\tilde{\varphi}}^{\text{LG}}(t_1)$ is given by:

$$\dot{\tilde{\varphi}}^{\text{LG}}(t_1) = \dot{Y}_{\tilde{\varphi}}(t_1) Y_{\tilde{\varphi}}(t_1)^\top + Y_{\tilde{\varphi}} \dot{Y}_{\tilde{\varphi}}(t_1)^\top.$$

Using the chain rule,

$$\dot{Y}_{\tilde{\varphi}}(t_1) = \frac{\partial Y_{\varphi}}{\partial t_1}(t_1) + \frac{\partial Y_{\varphi}}{\partial t_2}(t_2^*(t_1)) \dot{t}_2^*(t_1).$$

By the definition of $t_2^*(t_1)$, the term $\frac{\partial Y_{\varphi}}{\partial t_2}(t_2^*(t_1))$ is equal to zero. As a result, $\dot{Y}_{\tilde{\varphi}}(t_1) = \frac{\partial Y_{\varphi}}{\partial t_1}(t_1)$, which has been computed earlier.

References

- [1] P.-A. ABSIL, P.-Y. GOUSENBORGER, P. STRIEWSKI, AND B. WIRTH, *Differentiable piecewise-Bézier interpolation on Riemannian manifolds*, in Proceedings of the 26th European Symposium on Artificial Neural Networks, Computational Intelligence and Machine Learning (ESANN2016), Springer, 2016, pp. 95–100.
- [2] P.-A. ABSIL, P.-Y. GOUSENBORGER, P. STRIEWSKI, AND B. WIRTH, *Differentiable piecewise-Bézier surfaces on Riemannian manifolds*, SIAM Journal on Imaging Sciences, 9 (2016), pp. 1788–1828.

- [3] R. BERGMANN AND P.-Y. GOUSENBOURGER, *A variational model for data fitting on manifolds by minimizing the acceleration of a Bézier curve*, Frontiers in Applied Mathematics and Statistics, 4 (2018).
- [4] S. BONNABEL AND R. SEPULCHRE, *Riemannian metric and geometric mean for positive semidefinite matrices of fixed rank*, SIAM Journal on Matrix Analysis and Applications, 31 (2009), pp. 1055–1070.
- [5] N. BOUMAL AND P.-A. ABSIL, *A discrete regression method on manifolds and its application to data on $SO(n)$* , IFAC Proceedings Volumes (IFAC-PapersOnline), 44 (2011), pp. 2284–2289.
- [6] T. CAI AND W. LIU, *Adaptive thresholding for sparse covariance matrix estimation*, Journal of the American Statistical Association, 106 (2011), pp. 672–684.
- [7] T. CAI, W. LIU, AND X. LUO, *A constrained l_1 minimization approach to sparse precision matrix estimation*, Journal of the American Statistical Association, 106 (2011), pp. 594–607.
- [8] M. COCOCIONI, B. LAZZERINI, AND P. F. LERMUSIAUX, *Adaptive sampling using fleets of underwater gliders in the presence of fixed buoys using a constrained clustering algorithm*, in Proc. of OCEANS’15, Genova, Italy, May 18–21, 2015.
- [9] C. CONTI, M. COTRONEI, AND T. SAUER, *Full rank positive matrix symbols: interpolation and orthogonality*, BIT Numerical Mathematics, 48 (2008), pp. 5–27.
- [10] T. M. COVER AND J. A. THOMAS, *Elements of information theory*, John Wiley & Sons, 2012.
- [11] N. CRESSIE, *The origins of kriging*, Mathematical geology, 22 (1990), pp. 239–252.
- [12] N. CRESSIE, *Statistics for spatial data*, vol. 4, Wiley Online Library, 1992.
- [13] N. CRESSIE AND D. M. HAWKINS, *Robust estimation of the variogram*, Journal of the International Association for Mathematical Geology, 12 (1980), pp. 115–125.
- [14] N. CRESSIE AND H.-C. HUANG, *Classes of nonseparable, spatio-temporal stationary covariance functions*, Journal of the American Statistical Association, 94 (1999), pp. 1330–1339.
- [15] I. CSISZÁR, P. C. SHIELDS, ET AL., *Information theory and statistics: A tutorial*, Foundations and Trends in Communications and Information Theory, 1 (2004), pp. 417–528.
- [16] B. DOEKEMEIJER, S. BOERSMA, L. Y. PAO, AND J.-W. VAN WINGERDEN, *Ensemble Kalman filtering for wind field estimation in wind farms*, in 2017 American Control Conference (ACC), IEEE, 2017, pp. 19–24.
- [17] J. C. DRISCOLL AND A. C. KRAAY, *Consistent covariance matrix estimation with spatially dependent panel data*, Review of economics and statistics, 80 (1998), pp. 549–560.
- [18] J. FRIEDMAN, T. HASTIE, AND R. TIBSHIRANI, *Sparse inverse covariance estimation with the graphical lasso*, Biostatistics, 9 (2008), pp. 432–441.
- [19] R. FURRER, M. G. GENTON, AND D. NYCHKA, *Covariance tapering for interpolation of large spatial datasets*, Journal of Computational and Graphical Statistics, 15 (2006), pp. 502–523.

- [20] R. G. GALLAGER, *Information theory and reliable communication*, vol. 588, Springer, 1968.
- [21] P.-Y. GOUSENBOURGER, E. MASSART, AND P.-A. ABSIL, *Data fitting on manifolds with composite Bézier-like curves and blended cubic splines*, Journal of Mathematical Imaging and Vision, 61 (2018), pp. 645–671.
- [22] P.-Y. GOUSENBOURGER, E. MASSART, A. MUSOLAS, P.-A. ABSIL, L. JACQUES, J. M. HENDRICKX, AND Y. MARZOUK, *Piecewise-Bézier $C1$ smoothing on manifolds with application to wind field estimation*, in Proceedings of the 27th European Symposium on Artificial Neural Networks, Computational Intelligence and Machine Learning (ESANN2017), 2017, pp. 305–310.
- [23] J. R. GUERCI, *Theory and application of covariance matrix tapers for robust adaptive beam-forming*, IEEE Transactions on Signal Processing, 47 (1999), pp. 977–985.
- [24] R. GUHANIYOGI AND S. BANERJEE, *Multivariate spatial meta kriging*, Statistics & probability letters, 144 (2019), pp. 3–8.
- [25] J. HINKLE, P. T. FLETCHER, AND S. JOSHI, *Intrinsic polynomials for regression on Riemannian manifolds*, Journal of Mathematical Imaging and Vision, 50 (2014), pp. 32–52.
- [26] M. JOURNÉE, F. BACH, P.-A. ABSIL, AND R. SEPULCHRE, *Low-rank optimization on the cone of positive semidefinite matrices*, SIAM Journal on Optimization, 20 (2010), pp. 2327–2351.
- [27] A. KACEM, M. DAOUDI, B. BEN AMOR, S. BERRETTI, AND J. C. ALVAREZ-PAIVA, *A novel geometric framework on Gram matrix trajectories for human behavior understanding*, IEEE Transactions on Pattern Analysis and Machine Intelligence (T-PAMI), 42 (2018).
- [28] K.-R. KIM, I. L. DRYDEN, AND H. LE, *Smoothing splines on Riemannian manifolds, with applications to 3D shape space*, arXiv:1801.04978, (2018), pp. 1–23.
- [29] P. KUCHMENT, *An overview of periodic elliptic operators*, Bulletin of the American Mathematical Society, 53 (2016), pp. 343–414.
- [30] J. W. LANGELAAN, N. ALLEY, AND J. NEIDHOEFER, *Wind field estimation for small UAVs*, Journal of Guidance, Control, and Dynamics, 34 (2011), pp. 1016–1030.
- [31] J. W. LANGELAAN, J. SPLETZER, C. MONTELLA, AND J. GRENESTEDT, *Wind field estimation for autonomous dynamic soaring*, in Proceedings of the IEEE International Conference on Robotics and Automation (ICRA), 2012.
- [32] T. LARRABEE, H. CHAO, M. RHUDY, Y. GU, AND M. R. NAPOLITANO, *Wind field estimation in UAV formation flight*, in American Control Conference (ACC), 2014, IEEE, 2014, pp. 5408–5413.
- [33] N. LAWRENCE AND S. SUKKARIEH, *Simultaneous exploration and exploitation of a wind field for a small gliding UAV*, AIAA Guidance, Navigation and Control Conference, AIAA Paper, 8032 (2010).
- [34] N. R. LAWRENCE AND S. SUKKARIEH, *Path planning for autonomous soaring flight in dynamic wind fields*, in Proceedings of the IEEE International Conference on Robotics and Automation (ICRA), 2011, pp. 2499–2505.

- [35] O. LEDOIT AND M. WOLF, *A well-conditioned estimator for large-dimensional covariance matrices*, Journal of multivariate analysis, 88 (2004), pp. 365–411.
- [36] O. LEDOIT, M. WOLF, ET AL., *Nonlinear shrinkage estimation of large-dimensional covariance matrices*, The Annals of Statistics, 40 (2012), pp. 1024–1060.
- [37] O. LEDOIT, M. WOLF, ET AL., *Optimal estimation of a large-dimensional covariance matrix under Stein’s loss*, Bernoulli, 24 (2018), pp. 3791–3832.
- [38] X.-B. LI AND F. J. BURKOWSKI, *Conformational transitions and principal geodesic analysis on the positive semidefinite matrix manifold*, in Basu M., Pan Y., Wang J. (eds) Bioinformatics Research and Applications. ISBRA 2014. Lecture Notes in Computer Science, vol. 8492, Springer Cham, 2014, pp. 334–345.
- [39] J. LIU, J. HAN, Z.-J. ZHANG, AND J. LI, *Target detection exploiting covariance matrix structures in MIMO radar*, Signal Processing, 154 (2019), pp. 174–181.
- [40] T. LOLLA, P. HALEY JR, AND P. F. J. LERMUSIAUX, *Path planning in multi-scale ocean flows: Coordination and dynamic obstacles*, Ocean Modelling, 94 (2015), pp. 46–66.
- [41] E. MASSART AND P.-A. ABSIL, *Quotient geometry of the manifold of fixed-rank positive-semidefinite matrices*, SIAM J. Matrix Anal. Appl., 41 (2020), pp. 171–198.
- [42] E. MASSART, P.-Y. GOUSENBURGER, T. S. NGUYEN, T. STYKEL, AND P.-A. ABSIL, *Interpolation on the manifold of fixed-rank positive-semidefinite matrices for parametric model order reduction: preliminary results*, in Proceedings of the 27th European Symposium on Artificial Neural Networks, Computational Intelligence and Machine Learning (ESANN 2019), 2019, pp. 281–286.
- [43] V. MEHRMANN AND W. RATH, *Numerical methods for the computation of analytic singular value decompositions*, Electronic Transactions on Numerical Analysis, 1 (1993), pp. 72–88.
- [44] M. MOAKHER AND P. G. BATCHELOR, *Symmetric positive-definite matrices: From geometry to applications and visualization*, in Visualization and Processing of Tensor Fields, Springer, 2006, pp. 285–298.
- [45] K. MODIN, G. BOGFJELLMO, AND O. VERDIER, *Numerical Algorithm for C2-splines on symmetric spaces*, arXiv preprint arXiv:1703.09589, (2018).
- [46] A. MUSOLAS, S. T. SMITH, AND Y. MARZOUK, *Geodesically parameterized covariance estimation*, arXiv preprint arXiv:2001.01805, (2020).
- [47] D. S. OLIVER AND Y. CHEN, *Recent progress on reservoir history matching: a review*, Computational Geosciences, 15 (2011), pp. 185–221.
- [48] D. S. OLIVER, L. B. CUNHA, AND A. C. REYNOLDS, *Markov chain Monte Carlo methods for conditioning a permeability field to pressure data*, Mathematical Geology, 29 (1997), pp. 61–91.
- [49] H. J. PALANTHANDALAM-MADAPUSI, A. GIRARD, AND D. S. BERNSTEIN, *Wind-field reconstruction using flight data*, in 2008 American Control Conference, IEEE, 2008, pp. 1863–1868.
- [50] X. PENNEC, P. FILLARD, AND N. AYACHE, *A Riemannian framework for tensor computing*, International Journal of Computer Vision, 66 (2006), pp. 41–66.

- [51] C. E. RASMUSSEN, *Gaussian processes for machine learning*, MIT Press, 2006.
- [52] B. D. RIPLEY, *Spatial statistics*, vol. 575, John Wiley & Sons, 2005.
- [53] H. RUE AND L. HELD, *Gaussian Markov random fields: theory and applications*, CRC Press, 2005.
- [54] C. SAMIR, P.-A. ABSIL, A. SRIVASTAVA, AND E. KLASSEN, *A gradient-descent method for curve fitting on Riemannian manifolds*, Foundations of Computational Mathematics, 12 (2012), pp. 49–73.
- [55] J. SCHAFER AND K. STRIMMER, *A shrinkage approach to large-scale covariance matrix estimation and implications for functional genomics*, Applications in Genetics and Molecular Biology, 4 (2005), pp. 1175–1189.
- [56] M. L. STEIN, *Interpolation of spatial data: some theory for kriging*, Springer Science & Business Media, 2012.
- [57] M. L. STEIN, Z. CHI, AND L. J. WELTY, *Approximating likelihoods for large spatial data sets*, Journal of the Royal Statistical Society: Series B (Statistical Methodology), 66 (2004), pp. 275–296.
- [58] B. SZCZAPA, M. DAOUDI, S. BERRETTI, A. D. BIMBO, P. PALA, AND E. MASSART, *Fitting, Comparison, and Alignment of Trajectories on Positive Semi-Definite Matrices with Application to Action Recognition*, in Human Behavior Understanding, satellite workshop of the International Conf. on Computer Vision 2019 (ICCV2019), arxiv:1908.00646.
- [59] B. VANDEREYCKEN, P.-A. ABSIL, AND S. VANDEWALLE, *Embedded geometry of the set of symmetric positive semidefinite matrices of fixed rank*, in IEEE/SP 15th Workshop on Statistical Signal Processing, 2009, pp. 389–392.
- [60] B. VANDEREYCKEN, P.-A. ABSIL, AND S. VANDEWALLE, *A Riemannian geometry with complete geodesics for the set of positive semidefinite matrices of fixed rank*, IMA Journal of Numerical Analysis, (2012), pp. 481 – 514.
- [61] J. WOLFOWITZ ET AL., *The minimum distance method*, The Annals of Mathematical Statistics, 28 (1957), pp. 75–88.
- [62] S. YANG, N. WEI, S. JEON, R. BENCATEL, AND A. GIRARD, *Real-time optimal path planning and wind estimation using Gaussian process regression for precision airdrop*, in 2017 American Control Conference (ACC), IEEE, 2017, pp. 2582–2587.